How altering the modular architecture affects aspects of lectin activity: case study on human galectin-1

Tanja J. Kutzner[1], Adele Gabba[2], Forrest G. FitzGerald[3], Nadezhda V. Shilova[4], Gabriel García Caballero[1], Anna-Kristin Ludwig[1], Joachim C. Manning[1], Clemens Knospe[5], Herbert Kaltner[1], Fred Sinowatz[5], Paul V. Murphy[2,*], Mare Cudic[3,*], Nicolai V. Bovin[4,6,*], Hans-Joachim Gabius[1,*]

[1]Institute of Physiological Chemistry, Faculty of Veterinary Medicine, Ludwig-Maximilians-University Munich, 80539 Munich, Germany; [2]School of Chemistry, National University of Ireland, Galway, Ireland; [3]Department of Chemistry and Biochemistry, Florida Atlantic University, Boca Raton, FL 33431, USA; [4]Shemyakin-Ovchinnikov Institute of Bioorganic Chemistry, Russian Academy of Sciences, Laboratory of Carbohydrates, 117997 Moscow, Russia; [5]Institute of Anatomy, Histology and Embryology, Faculty of Veterinary Medicine, Ludwig-Maximilians-University Munich, 80539 Munich, Germany; [6]Centre for Kode Technology Innovation, School of Engineering, Computer & Mathematical Sciences, Auckland University of Technology, Auckland 1010, New Zealand

Running title

Design-activity relationships for galectin-1 and variants

Supplementary Material: 5 figures, 10 tables, available at:

https://syncandshare.lrz.de/dl/fiLLBPu53jYf1WftnKYbwttv/.zip

[*]to whom correspondence should be addressed:
Paul V. Murphy: Tel: +353 91 492 465, e-mail: paul.v.murphy@nuigalway.ie
Mare Cudic: Tel: +1 561 297 4645, Fax: +1 561 297 2759, e-mail: mcudic@fau.edu
Nicolai V. Bovin: Tel: +7 495 330 71 38, Fax: +7 495 330 55 92, e-mail: professorbovin@yandex.ru
H.-J. Gabius: Tel: +49 89 2180 2290, Fax: +49 89 2180 992290, e-mail: gabius@tiph.vetmed.uni-muenchen.de

Abstract

Discoveries on involvement of glycan-protein recognition in many (patho)physiological processes are directing attention to exploring the significance of a fundamental structural aspect of sugar receptors beyond glycan specificity, i.e. occurrence of distinct types of modular architecture. In order to trace clues for defining design-functionality relationships in human lectins, a lectin's structural unit has been used as source material for engineering custom-made variants of the wild-type protein. Their availability facilitates comparative analysis toward the stated aim. With adhesion/growth-regulatory human galectin-1 as example, the strategy of evaluating how changes of its design (here from the homodimer of non-covalently associated domains to i) linker-connected di- and tetramers and ii) a galectin-3-like protein) affect activity is illustrated by using three assay systems of increasing degree of glycan complexity. Whereas calorimetry with two cognate disaccharides and array testing with 647 (glyco)compounds disclosed no major changes, galectin histochemical staining profiles of tissue sections that present natural glycome complexity revealed differences between wild-type and linker-connected homo-oligomers as well as between the galectin-3-like variant and wild-type galectin-3 for cell-type positivity, level of intensity at the same site and susceptibility for inhibition by a bivalent glycocompound. These results underscore the strength of the documented approach. Moreover, they give direction to proceed to i) extending its application to other members of this lectin family, especially galectin-3, and ii) then analyzing impact of architectural alterations on cell surface lattice formation and ensuing biosignaling systematically, considering the variants' potential for translational medicine.

Key words: calorimetry / glycan / histochemistry / lectin / sugar code

Introduction

What distinguishes carbohydrates from the other alphabets of life (i.e. nucleotides and amino acids) is their ability to generate oligomers of unsurpassed coding capacity (Laine 1997; Schnaar 2015; Solís et al. 2015; Gabius and Roth 2017). Indeed, this chemical potential is turned into glycome complexity (Ginsburg and Neufeld 1969; Roth 1987; Brockhausen and Schachter 1997; Cummings 2009; Zuber and Roth 2009). As a consequence, proteins and sphingolipids can present a wide diversity of sugar-encoded signals (Buddecke 2009; Schengrund 2015; Corfield 2017; Kopitz 2017; Ledeen et al. 2018; Sandhoff et al. 2018). One route of the flow of this information toward eliciting effects is that these 'messages' are 'read' and then 'translated' by sugar receptors (lectins) (Gabius 2017; Manning et al. 2017a; Kaltner et al. 2018a). Their target (glycan) specificity and their modular architecture are assumed to be key factors that determine the profile of the functional outcome of glycan-lectin recognition. In fact, evolution has used ancestral lectin domains as source material to generate diversity on the levels of sequence and modular design. Along this line of reasoning, each type of design to present the common carbohydrate recognition domain (CRD) in a lectin family can be postulated to have its own characteristic mission. Intriguingly, not all theoretically possible modes of CRD arrangement are apparently realized in Nature, and, equally puzzling at present, differences in modular display within a lectin family exist for example between vertebrates and invertebrates. The fundamental issue on defining design-functionality relationships and the given open questions prompted us to perform this study.

Looking at adhesion/growth-regulatory galectins (Gals) as test case, the CRD is presented in three modes in vertebrates (Hirabayashi 1997; Cooper 2002; Kaltner et al. 2017; Manning et al. 2018a). As illustrated in Figure 1, the typical cross-linking (lattice-forming) activity of

galectins is made possible via different structural means: bivalency is attained by non-covalent or covalent (linker-dependent) association. The formation of CRD oligomers can alternatively involve a second type of module, i.e. an N-terminal tail (NT) with collagen-like repeats. Obviously, the restriction to the three types of design illustrated in Figure 1 poses the question as to why this particular set has phylogenetically become a stable trait in vertebrates. In order to resolve this issue, engineering of protein variants that display a distinct CRD in other types of design than the natural one enables to characterize the impact of altering CRD presentation on lectin properties.

Selecting homodimeric (proto-type) galectin-1 (Gal-1) for proof-of-principle work, the conversion of non-covalent association to covalent connection by short (Gly-Gly), flexible or rigid (α-helical) linkers (Bättig et al. 2004; Bi et al. 2008; Earl et al. 2011; Tribulatti et al. 2012; Vértesy et al. 2015), by disulfide bonding directed by a leucine zipper (van der Leij et al. 2007), by fusion of an immunoglobulin G_1 (IgG_1) F_c part to the CRD (Tsai et al. 2008; Cedeno-Laurent et al. 2010) and by site-specific (Cys130-dependent) self-conjugation of the Cys2Ser/Cys16Ser/Cys88Ser triple mutant using poly(ethylene glycol) diacrylate (Fettis and Hudalla 2018) led to bioactive homodimers. As predicted by studies using atomic force microscopy or glycodendrimersomes, the non-covalent association of this CRD appears to be more suited for *cis*-crosslinking and transient *trans*-bridging than for establishing firm contacts (Dettmann et al. 2000; Zhang et al. 2015). The insertion of a linker opens the route to generate homo-oligomers with the CRD of human Gal-1 beyond the dimer. Hereby, the artificial equivalent of the assumedly anti-microbial tandem-repeat-type oyster galectins, which are tetramers not found in vertebrates (Tasumi and Vasta 2007; Feng et al. 2013; 2015), became available (Kopitz et al. 2017). Equally important, a design switch between human galectins had recently been accomplished: Gal-1's CRD had been combined with the

NT of the chimera-type Gal-3 to turn homodimeric Gal-1 into a Gal-3-like Gal-1 variant termed Gal-3NT/1 (Ludwig et al. 2019a, b). Thus, rational engineering with the Gal-1 CRD has reached the status to facilitate comparative analysis of the wild-type protein *vs* variants of different design.

The selection of assay systems should consider the documented influence of the mode of glycan presentation, either free in solution (measured for example by frontal affinity chromatography or isothermal titration calorimetry, ITC) or on a solid phase/cell surface, on the extent of binding (Ahmad et al. 2002; Hirabayashi et al. 2002; Stowell et al. 2004, 2008; Leppänen et al. 2005; Song et al. 2009; Iwaki and Hirabayashi 2018). As consequence, protein design-ligand binding relationships were systematically determined in three assay systems: i) calorimetry to characterize the thermodynamics of binding the canonical ligands lactose (Lac) and N-acetyllactosamine (LacNAc), ii) glycan microarray monitoring and iii) galectin histochemistry on sections of two organs, i.e. murine epididymis and jejunum, that present characteristic, physiologically complex glycomes. By applying this experimental strategy, combining protein engineering with comparing activity profiles of the resulting proteins all built with the Gal-1 CRD as lectin part, the presented results provide insights into the effect of changes of modular design on aspects of lectin properties.

Results

The panel of Gal-1-based variants

Natural human Gal-1 is a homodimer non-covalently stabilized by mostly hydrophobic contacts of the CRD interfaces that appears to undergo monomerization from low-µM concentrations downward (Giudicelli et al. 1997; López-Lucendo et al. 2004; Stowell et al. 2009). Playing a modular puzzle with the human Gal-1 CRD as building block, five variants

were engineered by i) covalent conjugation of two or four Gal-1 CRDs using either the 33-amino-acid linker of human Gal-8 termed 8S (Figure 2, left) or the dipeptide Gly-Gly termed GG (Figure 2, center) to generate homodi- and tetramers (Figure 2, left and center) and ii) human Gal-3's NT as the second module (Figure 2, right). As a consequence, fundamental design switches originating from the proto-type structure are established (these basic structures are shown in Figure 1). These five proteins that share presence of the Gal-1 CRD could all be isolated by affinity chromatography on Lac-presenting beads, ascertaining their activity for binding the cognate disaccharide. They constitute the toolbox shown in Figure 2 to proceed to the comparative analysis with the wild-type protein, first by ITC.

Binding properties: ITC

Each protein was processed in the same experimental set-up using the common physiological target of the *ga*(lactose-binding)*lectins*, i.e. LacNAc, and also Lac. As exemplarily shown in Figure 3 for wild-type Gal-1, its GG-linked di- and tetramers as well as its Gal-3-like Gal-3NT/1 variant, injections of ligand-containing solution led to heat release, whose extent successively decreased as ligand concentration reached saturation. The calculated number of binding sites per protein (n) was invariably close to the expected values of 2 (for homodimers), 4 (for homotetramers) and 1 for the Gal-3-like monomer (Table I), fully in line with completely maintained lectin activity. As commonly reported for human galectins (e.g. by Dam et al. 2005), the binding process was enthalpically driven with a typical entropic penalty (Table I). This was also the case when using Lac as ligand, albeit at the known lower level of affinity (Supplementary data, Table SI).

Covalently connecting the two Gal-1 CRDs by bringing in a linker (either GG or 8S) and increasing the number of CRDs to form the tetramer may affect the avidity of consecutive

binding processes. As an indicator for cooperativity of binding of a monovalent ligand to a protein (complex) with at least two binding sites, Hill plots were derived from the ITC data and presented as log(concentration of free ligand) *vs* log(fraction of ligand-loaded galectin)/(fraction of ligand-free galectin). Together with the advantage of covering all available data by its logarithmic scaling in this type of plot, any (substantial) deviation from linearity (with a slope of 1.0) in the Hill plot will signal cooperativity of binding processes. The data obtained for the Gal-3NT/1 variant exemplarily illustrate the linearity of the Hill plot in the case of binding to a monovalent ligand, here LacNAc (Figure 4A). Fittingly, the tangent slopes of successively calculated 3-point intervals are around 1.0 throughout the titration (Figure 4B).

Applying this type of data processing to each case, the tabulated slope values were obtained. As summarized in Table I, they provide no robust evidence for cooperativity, considering deviations from normality mostly occurring at minimal changes of fractional occupancy, as shown in Supplementary data, Figure S1A,B, and the error brought in by Q subtraction. When running the titrations with this protein and Lac as ligand (independently up to 6 mM and 10 mM), slope values of 1.02 and 1.08, respectively, were obtained (Supplementary data, Figure S1C-F), as all other titrations with Lac (up to 14 mM for the 8S-linked tetramer) led to slope values close to 1 (Supplementary data, Table SI). These results document full loading of the proteins with ligand and a maintained thermodynamics with enthalpic gain as driving force for binding in each case. In addition, titrations with the GG-linked trimer and Lac (6 mM, 10 mM, 14 mM)/LacNAc (6 mM) consistently resulted in n-values close to 3, enthalpically driven thermodynamics and slope values close to 1 (Supplementary data, Tables SII/SIII). Hill plots therefore indicate no solid evidence for an occurrence of positive cooperativity by the structural remodeling of the dimer to tri- and tetramers. Moreover, computational

processing of data with the PEAQ software yielded fitting exclusively for the one-set-of-sites model.

In order to probe into binding properties of this panel for glycans beyond LacNAc when presented on a surface, each protein was biotinylated under activity-preserving conditions, then the proteins' Lac-inhibitable binding to surface-presented glycoprotein (asialofetuin) and to cells was ascertained and binding properties on a glycan microarray tested.

Binding properties: printed glycan array

The glycan array comprised a total of 647 printed substances encompassing glycocompounds (mono- to oligosaccharides and derivatives, glycopeptides, (lipo)polysaccharides and glycosaminoglycans) and peptides. Its capacity to delineate fine-specificity differences among closely related family members had previously been documented for chicken galectins (García Caballero et al. 2016) so that this test system was applied for this panel of proteins. With the exception of (biotinylated or fluorescent) wild-type Gal-1, all proteins proved active in this setting and gave graded signal profiles of binding, the intensity values recorded at the constant (mass) concentration of 50 µg/ml (please see Figure 5 for a side-by-side comparison; Supplementary data, Figure S2 for a bar graph; for complete listings of signal intensity, please see Supplementary data, Tables SIV-SIX).

In principle, LacNAc and its oligomers were found to be binding partners for the Gal-1-type CRD. Few major differences occurred between di- and tetramers, here the particularly strong signal intensity of LacNAc sulfated at two sites (3-O-SuGal and 6-O-Su-GlcNAc) when tested with the 8S-linked tetramer (Figure 5; Supplementary data, Figure S2). The broad-panel testing was also a means to answer the question on an influence of Gal-3's NT on ligand binding of the CRD of Gal-1, for example by the tail's backfolding or tendency for

aggregation. Affinity to internal (reducing-end) LacNAc units and the low-level recognition of the histo-blood group B tetrasaccharide clearly separate the proteins with the Gal-1 CRD, especially Gal-3-like Gal-3NT/1, from wild-type Gal-3 (Supplementary data, Figure S2). Obviously, these cases of glycans disclose that Gal-1's CRD rather maintains its binding pattern irrespective of the tested alterations of the protein architecture when interacting with surface-immobilized glycans in arrays. In order to take the test system from array-presented glycocompounds to cellular glycomes, tissue sections are an experimental platform that can trace differences up to the level of cell types. Of special note, in comparison to array-type presentation, the surface of tissue sections, by presenting physiologically complex glycomes, offers the naturally encountered possibility to bridge two structurally different binding partners for the cross-linking galectins.

Binding properties: galectin histochemistry

Glycophenotyping of sections of adult fixed murine epididymis and jejunum by plant, fungal and invertebrate lectins had indicated the suitability of these two organs for the given purpose (Lohr et al. 2010; Kaltner et al. 2018b). Sections of fixed tissues were processed first by controls to exclude signal generation in the absence of labelled galectin (Figure 6A; Supplementary data, Figure S3A) and to ascertain sensitivity of signal generation to presence of the cognate sugar (Figure 6B; Supplementary data, Figure S3B), then by titrations to determine the optimal concentration that avoids significant background staining for systematic comparisons. The distribution profiles of the galectin-dependent and Lac-inhibitable staining are summarized in Table II for the data on adult murine epididymis.

The overall quantitative differences of staining intensity seen between wild-type Gal-1 (yielding up to very strong (++++) intensity) and its covalently linked di- and tetrameric

variants (only reaching up to weak-level (+) intensity) in the cases of principal and apical but not basal cells (in this case, all proteins caused high (+++/++++) signal intensity) are illustrated in Figure 6B-F. High-magnification microphotographs substantiate the cell-type-dependent differences for comparisons of wild-type Gal-1 (Figure 6I, N, S) *vs* the GG-linked dimer (Figure 6J, O, T) or tetramer (Figure 6K, P, U). The similarity of staining profiles in signal distribution and intensity when testing Gal-1 and the Gal-3NT/1 variant, shown in Figure 6B, G, is documented in more detail in Figure 6I, N, S (Gal-1) and Figure 6L, Q, V (Gal-3NT/1). Since Gal-3 application led to reduced level of staining of principal and apical cells relative to the grade of intensity reached by the Gal-3-like Gal-1 variant (Table II, Figure 6H, M, R, W), the data of the galectin histochemical analysis were in line with the array-based results. In both cases, the nature of the CRD mattered in the two proteins of identical (chimera-type) design.

In order to answer the question on the possibility for observing differences by pairwisely analyzing staining profiles of labelled wild-type Gal-1 *vs* di- to tetramer and Gal-3NT/1 *vs* wild-type Gal-3 in cell types of other functionalities than reproduction, galectin histochemistry was performed in sections of adult murine jejunum. In principle, this appears to be the case (Supplementary data, Table SX). Strong intensity of staining of apical and supranuclear cytoplasm of surface enterocytes was obtained by labelled Gal-1 and its Gal-3NT/1 variant, whereas covalently linked di- and tetramers (exemplarily shown for the GG-linked dimer) and also wild-type Gal-3 reached comparatively lower intensity levels (Figure 7A, in clockwise representation; Supplementary data, Figure S3B-G for overviews and Figure S3I-L for enlarged details). The same congruence was seen for the neck of the epithelial lining, goblet cell staining revealing disparity among di- and tetramers, whereas the fundus, here Paneth cells, presents similarly strong intensity (Figure 7B, in clockwise representation;

Supplementary data, Figure S3B-G for overview and Figure S3N-Q for enlarged details). Again, the profile of staining by the Gal-3NT/1 variant could be distinguished from that of Gal-3 (Supplementary data, Figure S3G, H for overviews, Figure S3L, M, Q, R for enlarged details).

In addition to ascertaining binding by the canonical site of contact for Lac, as shown in the insets of Figure 6B and Supplementary data, Figure S3B, the inhibition assays were extended from using the cognate disaccharide to include synthetic neoglycoconjugates. They have the added value to serve as molecular rulers. The possibility for differential degrees of susceptibility to the presence of certain types of topological inhibitor presentation was examined with a pair of bi- and tetravalent compounds (Scheme 1). Bivalency of the Lac-presenting compound **1** is based on conjugation of sugar to a backbone with a stilbene residue (the synthetic route to its production shown in Scheme 2), whereas scaffold with a tetraphenylethylene established tetravalency for compound **2**. The types of central bridging lead to a distance of up to 33 Å for the two sugar units in the extended conformation of compound **1**, 18 Å, 28.5 Å and 32 Å separate the sugar headgroup at neighbouring and at opposing positions in compound **2**, as shown in Supplementary data, Figure S4 (all distances measured between the carbon atoms at the anomeric position of galactose as averages observed during 10-ns molecular dynamics runs). Crystal structures of substances with relaxed core point to the possibility either for a coplanar arrangement between phenyl rings and the alkene in bis(*p*-methoxy)-*trans*-stilbene (Theocharis et al. 1984) or for a lack of planarity between the phenyl ring and alkene in tetraphenylethene (Li et al. 2017). Conformational flexibility in other parts of the backbone can allow sugar headgroups to adopt a range of distances beyond those given in Supplementary data, Figure S4.

Testing sections of both organs systematically by titrations, the bivalent compound was clearly more effective than free Lac and Lac presented by the tetrameric scaffold. When concentrations were normalized for sugar content, reductions of staining when applying the labelled 8S-linked tetramer in a mixture with inhibitor on epididymis sections (Figure 8) and the GG-linked tetramer on jejunum sections (Supplementary data, Figure S5) back this statement. Remarkably, covalent association of the CRD caused increased degree of susceptibility to Lac-dependent inhibition of binding to sites in sections. The conjugation by insertion of the linker thus not only changes cellular aspects of binding profiles but also affects inhibitory potency of the cognate sugar, on sections of the tested organs processed by fixation especially for the bivalent compound. When testing the inhibitory capacity comparatively on native cell (CHO glycosylation mutant Lec8) surface binding, the signals were reduced rather similarly by the two synthetic compounds (not shown). Examining the natural chimera-type protein, valency of the scaffold affected Gal-3-dependent signal intensity more potently than it did for Gal-1-type proteins, in jejunum up to a 40-fold increase in inhibitory potency for both glycocompounds (not shown). Again, there is a difference between the two proteins with chimera-type design depending on the nature of the CRD, Gal-3 invariably being more sensitive to the presence of the two synthetic substances than Gal-3NT/1. The nature of origin of the CRD thus appears to matter for more aspects than glycan specificity.

Discussion

The basic structural unit of a lectin is defined by the folding around its contact site for the cognate ligand. The cooperation between glycan specificity and modular lectin design is assumed to ensure the apparently high selectivity for distinct counterreceptors (cellular glycoconjugates): this functional pairing underlies the accurate and efficient translation of

glycan-encoded messages (Gabius et al. 2016). Altering protein architecture can thus be an approach to delineate an influence of defined architecture variations on lectin activities and to open perspectives for examining translational biomedical applications of such variants of human lectins.

In this study, we used the CRD of human Gal-1 as a common platform to build a set of five variants shown in Figure 2. Two different lengths of linker were deliberately included, because anomalous scaling of diffusion coefficients in measurements on tandem-repeat-type galectins and a linkerless variant of Gal-4 by fluorescence correlation spectroscopy had taught the lesson on "counterintuitive consequences when simply considering molecular mass increase" (Göhler et al. 2010). Since Gal-3's trimodular design is unique among galectins (please see Figure 1), its CRD also being involved in homotypic interactions (Kuklinski and Probstmeier 1998; Yang et al. 1998; Lepur et al. 2012; Halimi et al. 2014; Ippel et al. 2016; Flores-Ibarra et al. 2018; Xiao et al. 2018), examining the Gal-3-like Gal-1 variant is supposed to probe into consequences of CRD substitution. At the same time, the Gal-1 CRD will attain monovalency, with potential for aggregation different from that of the wild-type protein.

Methodologically, we teamed up three types of assay to characterize binding properties. The first assay, i.e. ITC, informed us about affinity for Lac/LacNAc with enthalpic/entropic contributions and about the occurrence of cooperativity. Overall, the driving force for Lac/LacNAc invariably was the enthalpy gain and affinity values were rather similar. Covalent CRD association did not lead to cooperativity. No indication for cooperativity had been observed for LacNAc binding to homodimeric Gal-1, -2 and -7 and tandem-repeat-type Gal-4 (Dam et al. 2005), also seen with thiodigalactoside as ligand for Gal-4 (Martín-

Santamaría et al. 2011). Absence of deviation from linearity in Scatchard plots of binding of radiiodinated wild-type Gal-1 and the homo-oligomers to human (SK-N-MC) neuroblastoma cells adds evidence to a one-set-of-sites binding process (Kopitz et al. 1998, 2017). In contrast, marked negative cooperativity had been reported based on measurements from the perspective of loading of a multi(nona)valent ligand, i.e. the branch ends of the three complex-type N-glycans of asialofetuin, with galectin (Dam et al. 2005).

Proceeding from measurements with disaccharides in solution to monitoring specificity on a glycan array, rather similar profiles of signals were detected for the homo-oligomers. This result is in line with respective results obtained with the IgG_1 F_c part–Gal-1 CRD fusion proteins (Tsai et al. 2008; Cedeno-Laurent et al. 2010). It is thus not surprising that an 8S-linked Gal-1 homodimer did not acquire a new biological activity, i.e. to become an eosinophil chemoattractant as tandem-repeat-type Gal-9 is (Sato et al. 2002). Linker insertion therefore does not necessarily reprogram a galectin, although experience with a hexa(Gly)peptide in the place of the natural linker in Gal-8, leading to the statement that "it depends on the hinge" (Levy et al. 2006), advises to be cautious when considering extrapolation. The same applies to CRD conjugation with the NT of Gal-3. In comparison to wild-type Gal-3, the Gal-3NT/1 variant maintains the typical target specificity of Gal-1 to the terminal (non-reducing-end) position of LacNAc oligomers, whereas Gal-3 homes in on internal disaccharide units in polyLacNAc chains.

In order to take analysis from the glycan array a step closer to cellular relevance and to examine the physiological glycan complexity, we have added galectin histochemistry of tissue sections. They present complex glycomes and enable comparative monitoring on the level of various cell types. Testing revealed marked differences in signal intensities. Also,

sensitivity toward inhibition with cognate sugar, most effective with a bivalent glycocompound, was enhanced by linker insertion. The example of intramolecular bridging of contact sites in wheat germ agglutinin by a bivalent compound has taught the remarkable lesson that the synthetic scaffolds with conjugated Lac can be molecular rulers (Maierhofer et al. 2007; Schwefel et al. 2010; André et al. 2016). Indeed, spatial features of interplay between the Gal-1 CRDs in the wild-type protein and in the linker-connected variants and contact sites in sections appear to be non-uniform; the same applied to wild-type Gal-3 and Gal-3-like Gal-3NT/1, here likely also involving the individual characteristics of the interplay of CRD (Gal-1 or -3) with itself in intermolecular contacts and/or with the NT. Concerning binding of ligands in sections, similar staining profiles for the wild-type and Gal-3-like Gal-1 proteins were determined, as opposed to wild-type Gal-3. The cases of difference in staining profiles of epididymal principal/apical *vs* basal cells as well as subapical *vs* supranuclear cytoplasmatic positivity of surface enterocytes when working with wild-type Gal-1 and its covalently linked variants yet argue against simple extrapolations. Evidently, covalent CRD conjugation can modulate certain aspects of staining profiles in different manners.

In this sense, our report gives direction to broaden the study of variants and to define their properties in ligand recognition up to binding to cell surfaces and eliciting post-binding effects, starting with analyzing the spatial nature of galectin-induced lattices. After all, cross-linking of counterreceptors is assumed to be at the heart of galectin functionality (Brewer 2002; Boscher et al. 2011; Kasai 2018; Sato 2018). Considering antagonist activity of Gal-3 (and also the Gal-3NT/1 variant) on Gal-1 as negative neuroblastoma growth regulator (Kopitz et al. 2001; Ludwig et al. 2019a) and formation of cross-linked complexes with disparate structural organization together with Lac-bearing glycoclusters by these two proteins (Ahmad et al. 2004), lectin design apparently is a source for variability of functional

aspects. Further comparative analyses with wild-type and variant proteins, then also with a Gal-1-like Gal-3 homodimer (Ludwig et al. 2019a), can therefore provide hints to understand emerging aspects of expression of galectins as network (Manning et al. 2017b, 2018b; Zivicová et al. 2017) and of their emerging, likely clinically relevant networking (Weinmann et al. 2018). Such studies have potential to establish an innovative class of specific antagonist/effector proteins on the platform of human galectin domains with a perspective for testing clinical applicability.

Materials and methods

Protein production and labeling

The wild-type proteins and five variants were obtained by recombinant production, purified to homogeneity by affinity chromatography on home-made Lac-presenting resin and biotinylated under activity-preserving conditions using the N-hydroxysuccinimide ester derivative of biotin (Sigma, Munich, Germany), followed by routinely ascertaining maintained lectin activity, as described (Gabius et al. 1991; Kopitz et al. 2017; Ludwig et al. 2019a). In addition, the GG-linked homotrimer was produced, purified and characterized as described (Kopitz et al. 2017).

ITC measurements

Titrations were performed in 20 mM phosphate buffer (pH 7.2) containing 5 mM or 150 mM NaCl and 10 mM β-mercaptoethanol at constant temperature for the six proteins using a PEAQ-ITC (Malvern, Westborough, MA, USA) calorimeter, as described (Ludwig et al. 2019a). In brief, adding ligand stepwisely in 150 s intervals at 25 °C and 750 rpm in 2 µl aliquots of a 36.4 µl solution of 6 mM LacNAc/Lac (and 10 mM or 14 mM) to 200 µl galectin-containing solution (details on protein concentrations listed in Table I and

Supplementary data Table SI) in the calorimetric cell yielded measurements of heat release, respective data were processed by the MicroCal PEAQ-ITC Analysis software using a one-site model, and a fitted off-set parameter was applied to each titration to account for background. In the cases of Lac titrations, fixing the n-value at or near theoretical stoichiometry was applied, using lectin concentration of LacNAc titrations for parameter settings. Hill plot data analysis was performed, as applied for human galectins and a nonavalent ligand (asialofetuin) as described (Dam et al. 2005).

Array measurements

Biotinylated galectins were comparatively tested at the constant concentration of 50 µg/ml in phosphate buffered saline (PBS) containing 0.1% Tween-20, 1% bovine serum albumin and 0.01% NaN_3 for 1 h at 37 °C in a humidified chamber with the array slide presenting the panel of 647 (glyco)compounds, as described for chicken galectins (García Caballero et al. 2016). Glass surface had been pretreated with PBS containing 0.1% Tween-20 for 15 min to reduce background by non-specific protein adsorption. After thorough washing to remove unbound labelled protein, probing with fluorescent streptavidin (labelled with AlexaFluor®-555 dye; Molecular Probe, Eugene, USA) followed for 45 min at 20 °C. After thoroughly washing with PBS-0.001% Tween-20 and then with deionized water to remove the fluorescent sensor protein, slides were scanned on an InnoScan 1100 AL scanner (Innopsys, Carbonne, France) using an excitation wavelength of 543 nm at 10 µm resolution. The obtained data were processed using ScanArray Express 4.0 software and the fixed 70 µm-diameter circle method as well as Microsoft Excel. Six spots represented each compound on the array (details on nature of the 647 compounds given in Tables SIV-IX), and binding data are reported as median RFU (relative fluorescence units) of replicates. Median deviation was

measured as interquartile range. A signal, whose fluorescence intensity exceeded the background value by a factor of five, was considered to be significant.

Galectin histochemistry

Fresh tissue specimen of four six-week-old C57 BL/6 mice we fixed in Bouin's solution for 24 h, dehydrated by passing them through a series of solutions of increasing contents of ethanol, then isopropanol and finally xylene prior to embedding in paraffin wax at 61 °C. Sections mounted on Superfrost® plus glass slides (Menzel, Braunschweig, Germany) were processed by an optimized protocol ensuring minimal background with Vectastain® ABC Kit and Vector® Red reagents (Biozol, Eching, Germany) for staining, as described (Kaltner et al. 2018b). In the case of each protein, systematic titrations including blocking by cognate sugar were carried out to compare profiles and identify a concentration for comparative analysis in three to five independent series that covered the following ranges: 0.0625-4 µg/ml for wild-type Gal-1 and the pair of homodimeric variants, up to 1 µg/ml for the pair of homotetrameric variants, up to 0.5 µg/ml for the Gal-3NT/1 protein and 16 µg/ml for wild-type Gal-3. Of note, titrations covered equal mass and molar concentration for the wild-type *vs* variant pairs. Data acquisition and recording followed a routine protocol (Kaltner et al. 2018b), and semiquantitative grading of intensity of staining is given in the footnote of Table II.

Glycocompound synthesis

NMR spectra were recorded with 500 MHz & 600 MHz Varian spectrometers. Chemical shifts are reported relative to internal Me_4Si in $CDCl_3$ (δ 0.0), HOD for D_2O (δ 4.84) or CD_2HOD (δ 3.31) for ^1H and $CDCl_3$ (77.16) or CD_3OD (49.05) for ^{13}C. NMR spectra were processed and analysed using MestReNova software. ^1H NMR signals were assigned with the

aid of gCOSY. ^{13}C NMR signals were assigned with the aid of APT, gHSQCAD and/or gHMBCAD. Coupling constants are reported in Hertz. Low- and high-resolution mass spectra were measured on a Waters LCT Premier XE Spectrometer, measuring in both positive and/or negative mode as, using MeCN, H_2O and/or MeOH as solvent. Thin layer chromatography (TLC) was performed on aluminium sheets precoated with silica gel 60 (HF254, E. Merck) and spots visualized by UV and charring with H_2SO_4-EtOH (1:20), cerium molybdate, or phosphomolybdic acid stains. Flash chromatography was carried out with silica gel 60 (0.040-0.630 mm; E. Merck or Aldrich) and using a stepwise solvent polarity gradient (starting with the conditions indicated in each case and increasing the polarity as required) correlated with TLC mobility. Chromatography solvents, cyclohexane, EtOAc, CH_2Cl_2 and MeOH were used as obtained from suppliers (Fisher Scientific and Sigma-Aldrich). Solvents for reactions under anhydrous conditions were directly used as obtained from a Pure Solv™ Solvent Purification System.

To obtain (E)-1,2-bis(4-(prop-2-yn-1-yloxy)phenyl)ethane (**4**), compound **3** was prepared (Andrus et al. 2002). To **3** (2.50 g, 10.4 mmol) dissolved in CH_2Cl_2 (40 ml), which had been cooled in an ice-salt bath, was added, dropwise, a solution of boron tribromide in CH_2Cl_2 (39 ml of 1.0 M, 39 mmol). The solution was allowed to attain room temperature and was then stirred for 15 h. Water (35 ml) was added slowly, dropwise, with stirring. The organic solvent was removed under reduced pressure, the aqueous phase was extracted with EtOAc (3 x 30 ml), the combined organic phases were dried over Na_2SO_4 and the solvent removed under reduced pressure. Column chromatography (7:3, cyclohexane-EtOAc) gave the demethylated intermediate (2.1 g, 97%); ^1H NMR (500 MHz, DMSO-d_6) δ 7.33 (d, J = 8.7 Hz, 4H, aromatic H), 6.88 (s, 2H, alkene H), 6.72 (d, J = 8.6 Hz, 4H, aromatic H);^{13}C NMR (126 MHz, DMSO-d_6) δ = 157.2 (C), 129.0 (C), 127.8 (CH aromatic), 125.6 (CH, alkene), 115.9 (CH aromatic); ESI-HRMS calcd for $C_{14}H_{11}O_2$ 211.0759, found m/z 211.0702 $[M-H]^-$. To this

intermediate (2.1 g, 9.9 mmol) dissolved in dry DMF (300 ml) was added anhydrous potassium carbonate (11.0 g, 79.3 mmol). Propargyl bromide (80% in toluene, 4.8 ml, 55 mmol) was then added and the mixture was stirred for 14 h at 70 °C under a nitrogen atmosphere. The reaction was then cooled to room temperature and was diluted with CH_2Cl_2 (300 ml). This solution was washed with saturated NH_4Cl, with the aqueous layer being re-extracted with a further portion of CH_2Cl_2 (3 x 150 ml). The combined organic layers were then washed with water and dried over Na_2SO_4, solvent was removed at reduced pressure. Column chromatography (7:3, cyclohexane-EtOAc) gave the title compound (2.43 g, 85%); ^{1}H NMR (500 MHz, $CDCl_3$) δ 7.44 (d, J = 8.7 Hz, 4H, aromatic H), 6.97 (d, J = 8.7 Hz, 4H, aromatic H), 6.94 (s, 2H, alkene H), 4.71 (s, 4H, CH_2), 2.53 (s, 2H, alkyne H);^{13}C NMR (126 MHz, chloroform-d) δ = 157.4 (C), 131.3 (C), 127.4 (aromatic CH), 126.5 (alkene CH), 115.1 (aromatic CH), 75.6 (alkyne CH), 55.9 (CH_2); ES-HRMS calcd for $C_{20}H_{16}NaO_2$ 311.1048, found m/z 311.1052 $[M+Na]^+$.

To obtain glycocompound **1**, compound **5** was prepared as described (Leyden et al. 2009). To **4** (108 mg, 0.42 mmol) dissolved in degassed THF-H_2O (1:1, 6 ml) were added **5** (561 mg, 0.92 mmol), sodium ascorbate (49 mg, 0.25 mmol) and $Cu_2SO_4 \cdot 5H_2O$ (62 mg, 0.25 mmol). The reaction mixture was stirred under inert atmosphere in a microwave reactor at 50 °C (120 W) for 30 min. Tetrahydrofuran was then removed under reduced pressure followed by the dilution of the solution with CH_2Cl_2. This mixture was washed with water. The aqueous layer was re-extracted with a further portion of CH_2Cl_2. The combined organic layers were dried over Na_2SO_4 and the solvent was removed at reduced pressure. Chromatography (95:5, CH_2Cl_2-MeOH) gave the protected intermediate (600 mg, 89 %) as a colourless solid; ^{1}H NMR (500 MHz, chloroform-d) δ 7.78 (s, 2H, triazole H), 7.40 (d, J = 8.8 Hz, 4H, aromatic H), 6.94 (d, J = 8.8 Hz, 4H, aromatic H), 6.91 (s, 2H, alkene H), 5.83 (d, J = 9.1 Hz, 2H, H-1), 5.39 (overlapping signals, 4H), 5.35 (d, J = 3.4 Hz, 2H), 5.20 (s, 4H, CH_2), 5.12 (dd, J = 10.4,

7.9 Hz, 2H, H-2'), 4.96 (dd, 10.4, 3.4 Hz, 2H, H-3'), 4.52 (d, J = 7.9 Hz, 2H, H-1'), 4.47 (d, J = 11.0 Hz, 2H, H-6), 4.18 – 4.06 (overlapping signals, 6H, H-6 and H-6' protons), 3.98 – 3.83 (overlapping signals, 6H, H-4,H-5, H-5'), 2.15 (s, 6H, OAc), 2.09 (s, 6H, OAc), 2.06 (s, 6H, OAc), 2.05 (s, 6H, OAc), 2.04 (s, 6H, OAc), 1.96 (s, 6H, OAc), 1.82 (s, 6H, OAc); ^{13}C NMR (126 MHz, chloroform-d) δ = 170.3, 170.2, 170.1, 170.0, 169.4, 169.1, 169.0 (each C, each OAc), 157.5 (aromatic C), 144.8 (triazole C), 131.0 (aromatic C), 127.5 (aromatic CH), 126.3 (alkene CH), 121.1 (triazole CH), 115.0 (aromatic CH), 101.1 (CH, C-1'), 85.5(CH, C-1), 75.9 (CH, C-4), 75.6 (CH,C-5), 72.6 (CH,C-3), 70.9 (CH,C-3'), 70.8 (CH,C-2), 70.5 (CH,C-2'), 69.0, 66.6 (CH,C-4'), 61.9 (CH_2), 61.7(CH_2,C-6), 60.8 (CH_2,C-6'), 20.8 (CH_3, OAc), 20.7(CH_3, OAc), 20.6 (CH_3, OAc), 20.6 (CH_3, OAc), 20.6 (CH_3, OAc), 20.5(CH_3, OAc), 20.1(CH_3, OAc), ES-HRMS calcd for $C_{72}H_{86}N_6NaO_{36}$ 1633.4981, found m/z 1633.4985 $[M+Na]^+$. To a suspension of this intermediate (400 mg, 0,25 mmol) in dry MeOH (10 ml, cooled 0 °C), freshly prepared 1M NaOMe in MeOH was added until the solution reached pH 10. The reaction mixture was allowed to attain room temperature and stirred for 15 h. Glacial acetic acid was added to neutralise (pH = 7) the solution. [NOTE: it is possible to use Amberlite IR- 120 H+ instead of AcOH, but filtration is difficult due to the low solubility of **1**]. The solvent was removed under reduced pressure. Reverse phase column (three volumes of water were flushed through the column, to ensure salt removal, followed by a MeCN-H_2O mixture of 3:2 ratio) gave the title compound **1** as white solid (250 mg, 96%) [NOTE: the compound dissolves in a minimal volume of water with few drops of MeCN added. If the product precipitates, one drop of AcOH can be added and the mixture heated slightly to redissolve solid compound]; ^{1}H NMR (500 MHz, DMSO-d6) δ 8.46 (s, 2H, triazole H), 7.52 (d, J = 8.8 Hz, 4H, aromatic H), 7.11 – 7.00 (overlapping signals, 6H, aromatic H, alkene H), 5.67 (d, J = 9.3 Hz, 2H, H-1), 5.17 (s, 4H, CH_2), 4.26 (d, J = 7.9 Hz, 2H, H-1'), 3.87 (t, J = 9.3 Hz, 2H, H-2), 3.78 (d, J = 10.6 Hz, 2H ,H-6), 3.70 – 3.44 (overlapping signals, 16H), 3.42

– 3.29 (overlapping signals, 4H); ^{13}C NMR (126 MHz, DMSO-d6) δ 157.9 (C), 143.1 (C), 130.8 (C), 127.9 (CH, aromatic), 126.4 (CH, aromatic), 124.4 (CH, triazole), 115.3 (CH, aromatic), 104.2 (CH, C-1'), 87.4 (CH, C-1), 80.2 (CH), 78.2 (CH), 76.0 (CH), 75.6 (CH), 73.7 (CH), 72.2 (CH), 71.0 (CH), 68.6 (CH), 61.4 (CH_2), 60.9 (CH_2), 60.5 (CH_2); ES-HRMS calcd for $C_{44}H_{57}N_6O_{22}$ 1021.3526, found m/z 1021.3566 $[M-H]^-$

The tetraphenylene-based glycocompound **2** was prepared, as described and applied to lectin testing previously (Hu et al. 2011; André et al. 2015). Analytical data: ^{1}H NMR (500 MHz, DMSO-d6) δ 8.43 (s, 4H, triazole H), 6.90 (d, J = 8.5 Hz, 8H, aromatic H), 6.84 (d, J = 8.6 Hz, 8H, aromatic H), 5.66 (d, J = 9.3 Hz, 4H, H-1), 5.65 – 5.61 (overlapping signals, 4H, OH), 5.20 (br s, 4H, OH), 5.07 (s, 8H, CH_2), 4.95 (br s, 4H, OH), 4.92 (br s, 2H, OH), 4.75 – 4.65 (overlapping signals, 8H, OH), 4.59 (br s, 4H, OH), 4.26 (d, J = 7.1 Hz, 4H, H-1'), 3.87 (q, J = 8.9 Hz, 4H, H-2), 3.78 (t, J = 10.8, 4.9 Hz, 4H), 3.70 – 3.45 (overlapping signals, 34H), 3.40 – 3.33 (overlapping signals, 8H); ^{13}C NMR (126 MHz, DMSO-d6) δ 171.1 (C), 156.9 (C), 143.0 (C), 137.0 (C), 132.5 (CH, aromatic), 124.4 (CH, triazole), 114.3 (CH, aromatic), 104.2 (CH, C-1') , 87.4 (CH, C-1), 80.2 (CH), 78.2 (CH), 76.1(CH), 75.6 (CH), 73.7 (CH), 72.2 (CH, C-2), 71.0 (CH), 68.6 (CH_2), 60.9 (CH_2), 60.5 (CH_2); ES-HRMS calcd for $C_{86}H_{111}N_{12}O_{44}$ 2015.6817, found m/z 2015.6818 $[M-H]^-$.

Low-energy conformers of both glycocompounds were generated by molecular modeling applying structure building using Maestro version 6.0 (Schrodinger Inc., LLC, New York, USA) and energy minimization (OPLS-AA force field, GB/SA continuum solvation model for water (Still et al. 1990)) using Macromodel version 6.0.107 (Schrodinger Inc.), in part as described (Wang et al. 2012). Distances reported are averages obtained from 1000 structures sampled during 10-ns molecular dynamics simulations. The stochastic dynamics method was employed at a simulation temperature of 300 K, a time step of 1.5 fs and an equilibration time

of 1.0 ps. No constraints were imposed during the simulation in the case of compound **2**. In the case of substance **1**, the phenyl rings and alkene were constrained to match a coplanar arrangement.

Inhibitory capacity of glycocompounds

Systematic titrations with solutions containing free or glycocompound-presented Lac (all concentrations normalized to Lac) were performed in 2-fold serial dilutions in the range of 25 µM to 200 mM (Lac) or to 10 mM Lac (glycocompound). Solutions with biotinylated galectin and inhibitor were mixed and incubated for 1 h at room temperature, and pre-treated sections were exposed to aliquots of the mixture in parallel overnight at 4 °C together with mock-treated controls (=100%). All concentrations used for experiments of documented data are given in the legends of respective figures. Cytofluorometric analysis with fluorescent galectins and cells of the Chinese hamster ovary (CHO) glycosylation mutant Lec8 were carried out as described (André et al. 2016; Kopitz et al. 2017).

Acknowledgements

We gratefully acknowledge the excellent input provided by the reviewers, generous support by the Science Foundation Ireland grant 16/IA/4419 and the Irish Research Council grant GOIPG/2016/858 (to P. M. V.) and the NIH, National Cancer Institute grant R21-CA178754 (to M. C.) as well as inspiring discussions with Drs. B. Friday, A. Leddoz and A. W. L. Nose.

References

Ahmad N, Gabius H-J, Kaltner H, André S, Kuwabara I, Liu F-T, Oscarson S, Norberg T, Brewer CF. 2002. Thermodynamic binding studies of cell surface carbohydrate epitopes to galectins-1, -3 and -7. Evidence for differential binding specificities. *Can J Chem*. 80:1096-1104.

Ahmad N, Gabius H-J, André S, Kaltner H, Sabesan S, Roy R, Liu B, Macaluso F, Brewer CF. 2004. Galectin-3 precipitates as a pentamer with synthetic multivalent carbohydrates and forms heterogeneous cross-linked complexes. *J Biol Chem*. 279:10841-10847.

André S, O'Sullivan S, Koller C, Murphy PV, Gabius H-J. 2015. Bi- to tetravalent glycoclusters presenting GlcNAc/GalNAc as inhibitors: from plant agglutinins to human macrophage galactose-type lectin (CD301) and galectins. *Org Biomol Chem*. 13:4190-4203.

André S, Kaltner H, Kayser K, Murphy PV, Gabius H-J. 2016. Merging carbohydrate chemistry with lectin histochemistry to study inhibition of lectin binding by glycoclusters in the natural tissue context. *Histochem Cell Biol*. 145:185-199.

Andrus MB, Mendenhall KG, Meredith EL, Soma Sekhar BBV. 2002. Glycolate aldol reactions with boron enolates of bis-4-methoxyphenyl dioxanone. *Tetrahedron Lett*. 43:1789-1792.

Bättig P, Saudan P, Gunde T, Bachmann MF. 2004. Enhanced apoptotic activity of a structurally optimized form of galectin-1. *Mol Immunol*. 41:9-18.

Bi S, Earl LA, Jacobs L, Baum LG. 2008. Structural features of galectin-9 and galectin-1 that determine distinct T cell death pathways. *J Biol Chem*. 283:12248-12258.

Boscher C, Dennis JW, Nabi IR. 2011. Glycosylation, galectins and cellular signaling. *Curr Opin Cell Biol*. 23:383-392.

Brewer CF. 2002. Binding and cross-linking properties of galectins. *Biochim Biophys Acta*. 1572:255-262.

Brockhausen I, Schachter H. 1997. Glycosyltransferases involved in N- and O-glycan biosynthesis. In: Gabius H-J, Gabius S, editors. *Glycosciences: Status and Perspectives*. London - Weinheim: Chapman & Hall. p. 79-113.

Buddecke E. 2009. Proteoglycans. In: Gabius H-J, editor. *The Sugar Code. Fundamentals of glycosciences*. Weinheim, Germany: Wiley-VCH. p. 199-216.

Cedeno-Laurent F, Barthel SR, Opperman MJ, Lee DM, Clark RA, Dimitroff CJ. 2010. Development of a nascent galectin-1 chimeric molecule for studying the role of leukocyte galectin-1 ligands and immune disease modulation. *J Immunol*. 185:4659-4672.

Cooper DNW. 2002. Galectinomics: finding themes in complexity. *Biochim Biophys Acta*. 1572:209-231.

Corfield AP. 2017. Eukaryotic protein glycosylation: a primer for histochemists and cell biologists. *Histochem Cell Biol*. 147:119-147.

Cummings RD. 2009. The repertoire of glycan determinants in the human glycome. *Mol BioSyst*. 5:1087-1104.

Dam TK, Gabius H-J, André S, Kaltner H, Lensch M, Brewer CF. 2005. Galectins bind to the multivalent glycoprotein asialofetuin with enhanced affinities and a gradient of decreasing binding constants. *Biochemistry*. 44:12564-12571.

Dettmann W, Grandbois M, André S, Benoit M, Wehle AK, Kaltner H, Gabius H-J, Gaub HE. 2000. Differences in zero-force and force-driven kinetics of ligand dissociation

from β-galactoside-specific proteins (plant and animal lectins, immunoglobulin G) monitored by plasmon resonance and dynamic single molecule force microscopy. *Arch Biochem Biophys*. 383:157-170.
Earl LA, Bi S, Baum LG. 2011. Galectin multimerization and lattice formation are regulated by linker region structure. *Glycobiology*. 21:6-12.
Feng C, Ghosh A, Amin MN, Giomarelli B, Shridhar S, Banerjee A, Fernandez-Robledo JA, Bianchet MA, Wang LX, Wilson IB, *et al.* 2013. The galectin CvGal1 from the eastern oyster (*Crassostrea virginica*) binds to blood group A oligosaccharides on the hemocyte surface. *J Biol Chem*. 288:24394-24409.
Feng C, Ghosh A, Amin MN, Bachvaroff TR, Tasumi S, Pasek M, Banerjee A, Shridhar S, Wang LX, Bianchet MA, *et al.* 2015. Galectin CvGal2 from the Eastern oyster (*Crassostrea virginica*) displays unique specificity for ABH blood group oligosaccharides and differentially recognizes sympatric *Perkinsus* species. *Biochemistry*. 54:4711-4730.
Fettis MM, Hudalla GA. 2018. Engineering reactive oxygen species-resistant galectin-1 dimers with enhanced lectin activity. *Bioconjug Chem*. 29:2489-2496.
Flores-Ibarra A, Vértesy S, Medrano FJ, Gabius H-J, Romero A. 2018. Crystallization of a human galectin-3 variant with two ordered segments in the shortened N-terminal tail. *Sci Rep*. 8:9835.
Gabius H-J. 2017. How to crack the sugar code. *Folia Biol (Praha)*. 63:121-131.
Gabius H-J, Roth J. 2017. An introduction to the sugar code. *Histochem Cell Biol*. 147:111-117.
Gabius H-J, Wosgien B, Hendrys M, Bardosi A. 1991. Lectin localization in human nerve by biochemically defined lectin-binding glycoproteins, neoglycoprotein and lectin-specific antibody. *Histochemistry*. 95:269-277.
Gabius H-J, Manning JC, Kopitz J, André S, Kaltner H. 2016. Sweet complementarity: the functional pairing of glycans with lectins. *Cell Mol Life Sci*. 73:1989-2016.
García Caballero G, Kaltner H, Michalak M, Shilova N, Yegres M, André S, Ludwig A-K, Manning JC, Schmidt S, Schnölzer M, *et al.* 2016. Chicken GRIFIN: a homodimeric member of the galectin network with canonical properties and a unique expression profile. *Biochimie*. 128-129:34-47.
Ginsburg V, Neufeld EF. 1969. Complex heterosaccharides of animals. *Annu Rev Biochem*. 38:371-388.
Giudicelli V, Lutomski D, Levi-Strauss M, Bladier D, Joubert-Caron R, Caron M. 1997. Is human galectin-1 activity modulated by monomer/dimer equilibrium? *Glycobiology*. 7:viii-x.
Göhler A, André S, Kaltner H, Sauer M, Gabius H-J, Doose S. 2010. Hydrodynamic properties of human adhesion/growth-regulatory galectins studied by fluorescence correlation spectroscopy. *Biophys J*. 98:3044-3053.
Halimi H, Rigato A, Byrne D, Ferracci G, Sebban-Kreuzer C, ElAntak L, Guerlesquin F. 2014. Glycan dependence of galectin-3 self-association properties. *PLoS One*. 9:e111836.
Hirabayashi J, editor. 1997. Recent topics on galectins. *Trends Glycosci Glycotechnol*. 9:1-180.
Hirabayashi J, Hashidate T, Arata Y, Nishi N, Nakamura T, Hirashima M, Urashima T, Oka T, Futai M, Müller WEG, *et al.* 2002. Oligosaccharide specificity of galectins: a search by frontal affinity chromatography. *Biochim Biophys Acta*. 1572:232-254.
Hu XM, Chen Q, Wang JX, Cheng QY, Yan CG, Cao J, He YJ, Han BH. 2011. Tetraphenylethylene-based glycoconjugate as a fluorescence "turn-on" sensor for cholera toxin. *Chem Asian J*. 6:2376-2381.

Ippel H, Miller MC, Vértesy S, Zheng Y, Canada FJ, Suylen D, Umemoto K, Romano C, Hackeng T, Tai G, *et al.* 2016. Intra- and intermolecular interactions of human galectin-3: assessment by full-assignment-based NMR. *Glycobiology*. 26:888-903.
Iwaki J, Hirabayashi J. 2018. Carbohydrate-binding specificity of human galectins: an overview by frontal affinity chromatography. *Trends Glycosci Glycotechnol*. 30:SE137-SE153.
Kaltner H, Toegel S, García Caballero G, Manning JC, Ledeen RW, Gabius H-J. 2017. Galectins: their network and roles in immunity/tumor growth control. *Histochem Cell Biol*. 147:239-256.
Kaltner H, García Caballero G, Ludwig A-K, Manning JC, Gabius H-J. 2018a. From glycophenotyping by (plant) lectin histochemistry to defining functionality of glycans by pairing with endogenous lectins. *Histochem Cell Biol*. 149:547-568.
Kaltner H, Manning JC, García Caballero G, Di Salvo C, Gabba A, Romero-Hernández LL, Knospe C, Wu D, Daly HC, O'Shea DF, *et al.* 2018b. Revealing biomedically relevant cell and lectin type-dpendent structure-activity profiles for glycoclusters by using tissue sections as assay platform. *RSC Advances*. 8:28716-28735.
Kasai K-i. 2018. Galectins: quadruple-faced proteins. *Trends Glycosci Glycotechnol*. 30:SE221-SE223.
Kopitz J. 2017. Lipid glycosylation: a primer for histochemists and cell biologists. *Histochem Cell Biol*. 147:175-198.
Kopitz J, von Reitzenstein C, Burchert M, Cantz M, Gabius H-J. 1998. Galectin-1 is a major receptor for ganglioside GM1, a product of the growth-controlling activity of a cell surface ganglioside sialidase, on human neuroblastoma cells in culture. *J Biol Chem*. 273:11205-11211.
Kopitz J, von Reitzenstein C, André S, Kaltner H, Uhl J, Ehemann V, Cantz M, Gabius H-J. 2001. Negative regulation of neuroblastoma cell growth by carbohydrate-dependent surface binding of galectin-1 and functional divergence from galectin-3. *J Biol Chem*. 276:35917-35923.
Kopitz J, Xiao Q, Ludwig A-K, Romero A, Michalak M, Sherman SE, Zhou X, Dazen C, Vértesy S, Kaltner H, *et al.* 2017. Reaction of a programmable glycan presentation of glycodendrimersomes and cells with engineered human lectins to show the sugar functionality of the cell surface. *Angew Chem Int Ed*. 56:14677-14681.
Kuklinski S, Probstmeier R. 1998. Homophilic binding properties of galectin-3: involvement of the carbohydrate recognition domain. *J Neurochem*. 70:814-823.
Laine RA. 1997. The information-storing potential of the sugar code. In: Gabius H-J, Gabius S, editors. *Glycosciences: Status and Perspectives*. London - Weinheim: Chapman & Hall. p. 1-14.
Ledeen RW, Kopitz J, Abad-Rodríguez J, Gabius H-J. 2018. Glycan chains of gangliosides: functional ligands for tissue lectins (siglecs/galectins). *Progr Mol Biol Transl Sci*. 156:289-324.
Leppänen A, Stowell S, Blixt O, Cummings RD. 2005. Dimeric galectin-1 binds with high affinity to α2,3-sialylated and non-sialylated terminal N-acetyllactosamine units on surface-bound extended glycans. *J Biol Chem*. 280:5549-5562.
Lepur A, Salomonsson E, Nilsson UJ, Leffler H. 2012. Ligand induced galectin-3 protein self-association. *J Biol Chem*. 287:21751-21756.
Levy Y, Auslender S, Eisenstein M, Vidavski RR, Ronen D, Bershadsky AD, Zick Y. 2006. It depends on the hinge: a structure-functional analysis of galectin-8, a tandem-repeat type lectin. *Glycobiology*. 16:463-746.
Leyden R, Velasco-Torrijos T, André S, Gouin S, Gabius H-J, Murphy PV. 2009. Synthesis of bivalent lactosides based on terephthalamide, N,N'-diglucosylterephthalamide, and

glycophane scaffolds and assessment of their inhibitory capacity on medically relevant lectins. *J Org Chem*. 74:9010-9026.
Li D, Hu R, Guo D, Zang Q, Li J, Wang Y, Zheng Y-S, Tang BZ, Zhang H. 2017. Diagnostic absolute configuration determination of tetraphenylethene core-based chiral aggregation-induced emission compounds: particular fingerprint bands in comprehensive chiroptical spectroscopy. *J Phys Chem C*. 21:20947-20954.
Lohr M, Kaltner H, Schwartz-Albiez R, Sinowatz F, Gabius H-J. 2010. Towards functional glycomics by lectin histochemistry: strategic probe selection to monitor core and branch-end substitutions and detection of cell-type and regional selectivity in adult mouse testis and epididymis. *Anat Histol Embryol*. 39:481-493.
López-Lucendo MF, Solís D, André S, Hirabayashi J, Kasai K-i, Kaltner H, Gabius H-J, Romero A. 2004. Growth-regulatory human galectin-1: crystallographic characterisation of the structural changes induced by single-site mutations and their impact on the thermodynamics of ligand binding. *J Mol Biol*. 343:957-970.
Ludwig A-K, Michalak M, Xiao Q, Gilles U, Medrano FJ, Ma H, FitzGerald FG, Hasley WD, Melendez-Davila AM, Liu M, *et al.* 2019a. Design-functionality relationships for adhesion/growth-regulatory galectins. *Proc Natl Acad Sci USA*. 116:2837-2842.
Ludwig A-K, Kaltner H, Kopitz J, Gabius H-J. 2019b. Lectinology 4.0: Altering modular (ga)lectin display for functional analysis and biomedical applications. *Biochim Biophys Acta*. 1863:935-940.
Maierhofer C, Rohmer K, Wittmann V. 2007. Probing multivalent carbohydrate-lectin interactions by an enzyme-linked lectin assay employing covalently immobilized carbohydrates. *Bioorg Med Chem*. 15:7661-7676.
Manning JC, Romero A, Habermann FA, García Caballero G, Kaltner H, Gabius H-J. 2017a. Lectins: a primer for histochemists and cell biologists. *Histochem Cell Biol*. 147:199-222.
Manning JC, García Caballero G, Knospe C, Kaltner H, Gabius H-J. 2017b. Network analysis of adhesion/growth-regulatory galectins and their binding sites in adult chicken retina and choroid. *J Anat*. 231:23-37.
Manning JC, García Caballero G, Ruiz FM, Romero A, Kaltner H, Gabius H-J. 2018a. Members of the galectin network with deviations from the canonical sequence signature, 2. *G*alectin-*r*elated *p*rotein (GRP). *Trends Glycosci Glycotechnol*. 30:SE11-SE20.
Manning JC, García Caballero G, Knospe C, Kaltner H, Gabius H-J. 2018b. Three-step monitoring of glycan and galectin profiles in the anterior segment of the adult chicken eye. *Ann Anat*. 217:66-81.
Martín-Santamaría S, André S, Buzamet E, Caraballo R, Fernández-Cureses G, Morando M, Ribeiro JP, Ramirez-Gualito K, de Pascual-Teresa B, Cañada FJ, *et al.* 2011. Symmetric dithiodigalactoside: strategic combination of binding studies and detection of selectivity between a plant toxin and human lectins. *Org Biomol Chem*. 9:5445-5455.
Roth J. 1987. Subcellular organization of glycosylation in mammalian cells. *Biochim Biophys Acta*. 906:405-436.
Sandhoff R, Schulze H, Sandhoff K. 2018. Ganglioside metabolism in health and disease. *Progr Mol Biol Transl Sci*. 156:1-62.
Sato M, Nishi N, Shoji H, Seki M, Hashidate T, Hirabayashi J, Kasai K-i, Hata Y, Suzuki S, Hirashima M, *et al.* 2002. Functional analysis of the carbohydrate recognition domains and a linker peptide of galectin-9 as to eosinophil chemoattractant activity. *Glycobiology*. 12:191-197.

Sato S. 2018. Cytosolic galectins and their release and roles as carbohydrate-binding proteins in host-pathogen interaction. *Trends Glycosci Glycotechnol*. 30:SE129-SE135.
Schengrund C-L. 2015. Gangliosides: glycosphingolipids essential for normal neural development and function. *Trends Biochem Sci*. 40:397-406.
Schnaar RL. 2015. Glycans and glycan-binding proteins in immune regulation: a concise introduction to glycobiology for the allergist. *J Allergy Clin Immunol*. 135:609-615.
Schwefel D, Maierhofer C, Beck JG, Seeberger S, Diederichs K, Moller HM, Welte W, Wittmann V. 2010. Structural basis of multivalent binding to wheat germ agglutinin. *J Am Chem Soc*. 132:8704-8719.
Solís D, Bovin NV, Davis AP, Jiménez-Barbero J, Romero A, Roy R, Smetana K Jr, Gabius H-J. 2015. A guide into glycosciences: how chemistry, biochemistry and biology cooperate to crack the sugar code. *Biochim Biophys Acta*. 1850:186-235.
Song X, Xia B, Stowell SR, Lasanajak Y, Smith DF, Cummings RD. 2009. Novel fluorescent glycan microarray strategy reveals ligands for galectins. *Chem Biol*. 16:36-47.
Still WC, Tempczyk A, Hawley RC, Handrickson T. 1990. Semianalytical treatment of solvation for molecular mechanics and dynamics. *J Am Chem Soc.* 112:6127-6129.
Stowell SR, Dias-Baruffi M, Penttila L, Renkonen O, Nyame AK, Cummings RD. 2004. Human galectin-1 recognition of poly-N-acetyllactosamine and chimeric polysaccharides. *Glycobiology*. 14:157-167.
Stowell SR, Arthur CM, Mehta P, Slanina KA, Blixt O, Leffler H, Smith DF, Cummings RD. 2008. Galectin-1, -2, and -3 exhibit differential recognition of sialylated glycans and blood group antigens. *J Biol Chem*. 283:10109-10123.
Stowell SR, Cho M, Feasley CL, Arthur CM, Song X, Colucci JK, Karmakar S, Mehta P, Dias-Baruffi M, McEver RP, Cummings RD. 2009. Ligand reduces galectin-1 sensitivity to oxidative inactivation by enhancing dimer formation. *J Biol Chem.* 284: 4989-4999.
Tasumi S, Vasta GR. 2007. A galectin of unique domain organization from hemocytes of the Eastern oyster (*Crassostrea virginica*) is a receptor for the protistan parasite *Perkinsus marinus*. *J Immunol*. 179:3086-3098.
Theocharis CR, Jones W, Ramachandra Rao CN. 1984. An unusual photo-induced conformational polymorphism: a crystallographic study of bis(p-methoxy)-*trans*-stilbene. *J Chem Soc, Chem Commun*. 1291-1293.
Tribulatti MV, Figini MG, Carabelli J, Cattaneo V, Campetella O. 2012. Redundant and antagonistic functions of galectins-1, -3, and -8 in the elicitation of T cell responses. *J Immunol*. 188:2991-2999.
Tsai C-M, Chiu Y-K, Hsu T-L, Lin I-Y, Hsieh S-L, Lin K-I. 2008. Galectin-1 promotes immunoglobulin production during plasma cell differentiation. *J Immunol*. 181:4570-4579.
van der Leij J, van den Berg A, Harms G, Eschbach H, Vos H, Zwiers P, van Weeghel R, Groen H, Poppema S, Visser L. 2007. Strongly enhanced IL-10 production using stable galectin-1 homodimers. *Mol Immunol*. 44:506-513.
Vértesy S, Michalak M, Miller MC, Schnölzer M, André S, Kopitz J, Mayo KH, Gabius H-J. 2015. Structural significance of galectin design: impairment of homodimer stability by linker insertion and partial reversion by ligand presence. *Protein Eng Des Sel*. 28:199-210.
Wang G-N, André S, Gabius H-J, Murphy PV. 2012. Bi- to tetravalent glycoclusters: synthesis, structure-activity profiles as lectin inhibitors and impact of combining both valency and headgroup tailoring on selectivity. *Org Biomol Chem*. 10:6893-6907.
Weinmann D, Kenn M, Schmidt S, Schmidt K, Walzer SM, Kubista B, Windhager R, Schreiner W, Toegel S, Gabius H-J. 2018. Galectin-8 induces functional disease

markers in human osteoarthritis and cooperates with galectins-1 and -3. *Cell Mol Life Sci*. 75:4187-4205.
Xiao Q, Ludwig A-K, Romano C, Buzzacchera I, Sherman SE, Vetro M, Vértesy S, Kaltner H, Reed EH, Möller M, Wilson CJ, Hammer DA, Oscarson S, Klein ML, Gabius H-J, Percec V. 2018. Exploring functional pairing between surface glycoconjugates and human galectins using programmable glycodendrimersomes. *Proc Natl Acad Sci USA.* 115: E2509-E2518.
Yang R-Y, Hill PN, Hsu DK, Liu F-T. 1998. Role of the carboxyl-terminal lectin domain in self-association of galectin-3. *Biochemistry*. 37:4086-4092.
Zhang S, Moussodia R-O, Murzeau C, Sun HJ, Klein ML, Vértesy S, André S, Roy R, Gabius H-J, Percec V. 2015. Dissecting molecular aspects of cell interactions using glycodendrimersomes with programmable glycan presentation and engineered human lectins. *Angew Chem Int Ed*. 54:4036-4040.
Zivicová V, Broz P, Fík Z, Mifková A, Plzák J, Cada Z, Kaltner H, Kucerová JF, Gabius H-J, Smetana K, Jr. 2017. Genome-wide expression profiling (with focus on the galectin network) in tumor, transition zone and normal tissue of head and neck cancer: marked differences between individual patients and the site of specimen origin. *Anticancer Res*. 37:2275-2288.
Zuber C, Roth J. 2009. *N*-Glycosylation. In: Gabius H-J, editor. *The Sugar Code. Fundamentals of glycosciences*. Weinheim, Germany: Wiley-VCH. p. 87-110.

Legends to Figures

Fig. 1. Illustration of the three types of modular design of vertebrate galectins, i.e. proto-type (non-covalent association of two identical CRDs as in Gal-1), tandem-repeat-type (two different covalently connected CRDs, in human Gal-8 either by the short (S) 33-amino-acid linker (or by) its longer version (L; 74 amino acids)) and chimera-type (a CRD conjugated to an N-terminal tail (NT) composed of a peptide with two (Ser) sites for phosphorylation and non-triple helical collagen-like repeats, nine in human Gal-3) proteins (from top to bottom).

Fig. 2. Illustration of the routes of modular engineering to turn the CRD of Gal-1 into covalently associated homodi- and tetramers by linker insertion (left: 33-amino-acid linker of human Gal-8 shown in Figure 1; center: Gly-Gly) and into a Gal-3-like variant by bringing it together with Gal-3's NT thus termed Gal-3NT/1 (right). Color coding is used as in Figure 1.

Fig. 3. Illustration of the pair of thermogram (top) and isotherm (bottom) for the titration of galectin-containing solution in phosphate buffer (pH 7.2) containing 5 mM or 150 mM NaCl and 10 mM β-mercaptoethanol with 2 µl aliquots of a 6 mM LacNAc-containing solution in 150 s intervals at 25 °C in the cases of wild-type Gal-1 (**A**), the GG-linked homodimer (**B**), the GG-linked homotetramer (**C**) and the Gal-3NT/1 variant (**D**).

Fig. 4. Illustration of the Hill plot of the ITC data for LacNAc (6 mM) binding to Gal-3NT/1 (please see Figure 3D) at functional valency of 1 (**A**) and the corresponding bar graph of 3-point tangent slope data in the course of the titration (**B**).

Fig. 5. Illustration of side-by-side comparisons of relative signal intensity of galectin binding to selected glycans within the 647-compound-based array.

Fig. 6. Staining profiles obtained with the six biotinylated galectin proteins in cross sections through the initial segment of fixed murine epididymis. (**A**-**H**) Microphotographs present overviews with higher-level magnifications of distinct regions (inserted circle above the respective area including principal (p), apical (arrow) and basal cells (arrowhead)). (**I**-**W**) Moreover, enlarged views on these distinct cell types (i.e. principal cells (p), **I**-**M**; apical cells (arrows), **N**-**R**; basal cells (arrowheads), **S**-**W**) are given. (**A**) Negative control by omission of the incubation step with first-step reagent (labelled galectin) to exclude lectin-independent signal generation. (**B**) Strong binding of Gal-1 in the epithelial lining and comparatively weaker positivity in stereocilia (asterisk). Inset to **B** shows extent of reduction of galectin binding by co-incubation of labelled Gal-1 with Lac (200 mM). (**C**-**F**) Variants stained cytoplasm of epithelial cells, particularly strong in basal cells. In principal and apical cells, intensity was moderate for $(Gal\text{-}1)_2$-GG (**C**) and for $(Gal\text{-}1)_2$-8S (**D**) or weak ($(Gal\text{-}1)_4$-GG

(**E**). No staining was detected in the case of $(Gal\text{-}1)_4$-8S (**F**). Presence of 10 mM Lac completely inhibited binding of $(Gal\text{-}1)_4$-8S (inset to **F**; please see also Figure 8A, B). (**G**) Labelled Gal-3NT/1 generated a staining profile and degree of intensity comparable to Gal-1 (**B**), whereas binding sites for Gal-3 were detected at moderate intensity of staining supranuclearly (asterisk) in principal cells and at very strong intensity in basal cells (**H**). Enlarged views of the three main cell types (please see corresponding encircled areas in **B**-**H**) document nearly identical staining profiles for principal (p, **I**-**M**) and apical cells (arrows, **N**-**R**), except for a slightly stronger staining in the supranuclear cytoplasm of apical cells (asterisks). Incubations with labelled Gal-1 or Gal-3NT/1 led to strong and rather homogeneous staining of cytoplasm of principal (**I**, **L**) and of apical cells (**N**, **Q**). Weak staining intensity of principal and apical cells by the two variants $(Gal\text{-}1)_2$-GG (**J**, **O**) and $(Gal\text{-}1)_2$-8S (insets to **J** and **O**) as well as at best very weak staining by $(Gal\text{-}1)_4$-GG (**K**, **P**) and $(Gal\text{-}1)_4$-8S (insets to **K** and **P**) was recorded. Gal-3 binding was detected in apical and basal cytoplasm of both cell types (**M**, **R**) and, with moderate intensity, supranuclearly in principal cells (**M**, asterisk). (**S**-**W**) Basal cells were positive after processing of sections with labelled $(Gal\text{-}1)_2$-GG (**T**), $(Gal\text{-}1)_2$-8S (inset to **T**), $(Gal\text{-}1)_4$-GG (**U**), $(Gal\text{-}1)_4$-8S (inset to **U**) and Gal-3 (**W**). Processing with labelled Gal-1 (**S**) or Gal-3NT/1 (**V**) resulted in staining intensity of basal cells, which was not different from that of principal and apical cells. The following concentrations were applied: Gal-1, $(Gal\text{-}1)_2$-GG, $(Gal\text{-}1)_2$-8S, $(Gal\text{-}1)_4$-GG, $(Gal\text{-}1)_4$-8S, Gal-3NT/1: 0.5 µg/ml; Gal-3: 8.0 µg/ml. Scale bars are 50 µm (**A-H,** bottom right insets in **B**, **F**) or 5 µm (circles in **B**-**H**, **I**-**W**).

Fig. 7. Enlarged views of discriminatory aspects of the staining patterns of Gal-1, $(Gal\text{-}1)_2$-GG and Gal-3NT/1 in villi enterocytes (**A**) and of Gal-1, $(Gal\text{-}1)_2$-8S and Gal-3NT/1 in the fundus of epithelial lining of crypts (**B**) in sections of fixed murine jejunum.

Microphotographs are presented in a clockwise manner. (**A**) Strong cytoplasmatic staining of surface enterocytes by Gal-1 and moderate supranuclear (arrowhead) staining by $(Gal\text{-}1)_2$-GG. The staining profile by Gal-3NT/1 was nearly identical to that of Gal-1. The brush border (bb) was moderately positive with Gal-1 and Gal-3NT/1, weakly with $(Gal\text{-}1)_2$-GG. Contents of goblet cells (arrows) was invariably negative. (**B**) Strong positivity cytoplasmatically in precursors of enterocytes (asterisks), of goblet cells (arrowheads, contents was negative) and of crypt-associated cells (arrows) such as enteroendocrine cells and Paneth cells was obtained with Gal-1, very strong with $(Gal\text{-}1)_2$-8S in crypt-associated cells only. Profile of Gal-3NT/1 staining was similar to that of Gal-1. The concentration of probe was constant at 0.25 µg/ml. Scale bars are 5 µm (**A**) and 10 µm (**B**).

Fig. 8. Effect of increasing concentrations of cognate sugar (Lac) added free in solution or as part of the two glycocompounds on the staining profile obtained with biotinylated $(Gal\text{-}1)_4$-8S in cross sections through the initial segment of fixed murine epididymis. The signal remained at near to 100% level in the presence of 0.025 mM Lac tested as free sugar (**A**) or presented either by tetravalent compound **2** (inset to **A**) or bivalent compound **1** (**C**). Increasing the sugar concentration to 0.5 mM free Lac (**B**; please also see complete inhibition by 10 mM Lac in Fig. 6 inset to F) and scaffold-presented Lac by tetravalent compound **2** (inset to **B**) reduced staining intensity by 1-2 categories in the semiquantitative ranking (from ++++ to ++/+++) and number of positive basal cells by approximately 20%. In stark contrast, presence of compound **1** at this concentration precluded any binding of galectin (**D**). Symbols for semiquantitative grading of staining intensity are given in the rectangular box in the top-right area of each microphotograph and inset (for correlation of symbols to staining intensity, please see footnote in Table II). Scale bars are 50 µm. $(Gal\text{-}1)_4$-8S was applied at a concentration of 0.5 µg/ml.

Legends to Schemes

Scheme 1. Structural illustrations of the stilbene-based bivalent compound **1** and the tetraphenylethylene-based tetravalent compound **2**.

Scheme 2. Route of synthesis of the bivalent compound **1**.

Table I. Thermodynamic parameters and Hill coefficients of binding of LacNAc (6 mM) to human galectins at 25 °C

Cell	[Cell] (μM)	K_a ($x10^4$ M^{-1})	-ΔG (kcal/mol)	-ΔH (kcal/mol)	-TΔS (kcal/mol)	n (sites/protein)	K_d (μM)	Hill coefficient[a]
Gal-1	110	1.17	5.55	9.81 (± 0.083)	4.26	2.09	85.2 (± 1.52)	1.10
$(Gal\text{-}1)_2$-GG	95	1.99	5.88	9.15 (± 0.220)	3.27	1.96	50.1 (± 2.96)	1.09
$(Gal\text{-}1)_2$-8S	95	1.10	5.51	10.8 (± 0.122)	5.29	1.98	90.9 (± 1.78)	1.069
$(Gal\text{-}1)_4$-GG	50	1.99	5.87	8.78 (± 0.188)	2.91	3.97	50.2 (± 2.75)	1.15
$(Gal\text{-}1)_4$-8S	34	1.12	5.52	10.1 (± 0.267)	4.58	4.06	89.5 (± 3.14)	1.09
Gal-3NT/1	70	0.74	5.27	11.8 (± 0.081)	6.53	0.98	136 (± 1.63)	0.980

[a] obtained from successive 3-point tangent slope at y=0.

Table II. Distribution and cellular localization of galectin-dependent and Lac-inhibitable staining in sections of fixed adult murine epididymis[a]

type of protein / site of staining	Gal-1	$(Gal\text{-}1)_2$-GG	$(Gal\text{-}1)_2$-8S	$(Gal\text{-}1)_4$-GG	$(Gal\text{-}1)_4$-8S	Gal-3NT/1	Gal-3
principal cells							
stereocilia	++	-/+	-/+	-	-	(+)	-/+
apical[b]	++++	+/++	+/++	(+)	-/+	++++	+
supranuclear[b]	++++	+/++	+/++	(+)	-/+	++++	++
basal[b]	++++	(+)	(+)	(+)	-/+	++++	+
apical cells	++++	+/++[c]	+/++[c]	-/(+)[c]	-/(+)[c]	++++	+/++[c]
basal cells	++++	+++	++++	++++	++++	++++	++++
smooth muscle cells	-	-	-	-	-	-	-
connective tissue	-	-	-	+	+	-	-

[a] intensity of staining in sections is grouped into the following categories: -, no staining; (+), very weak but above background; +, weak; ++, medium; +++, strong; ++++, very strong.
[b] positivity of given regions of cytoplasm.
[c] staining intensity of supranuclear cytoplasm of apical cells consistently in higher category.

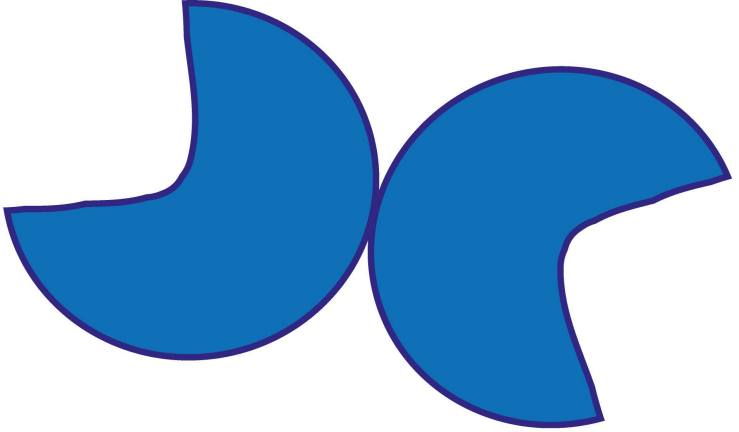

Gal-1

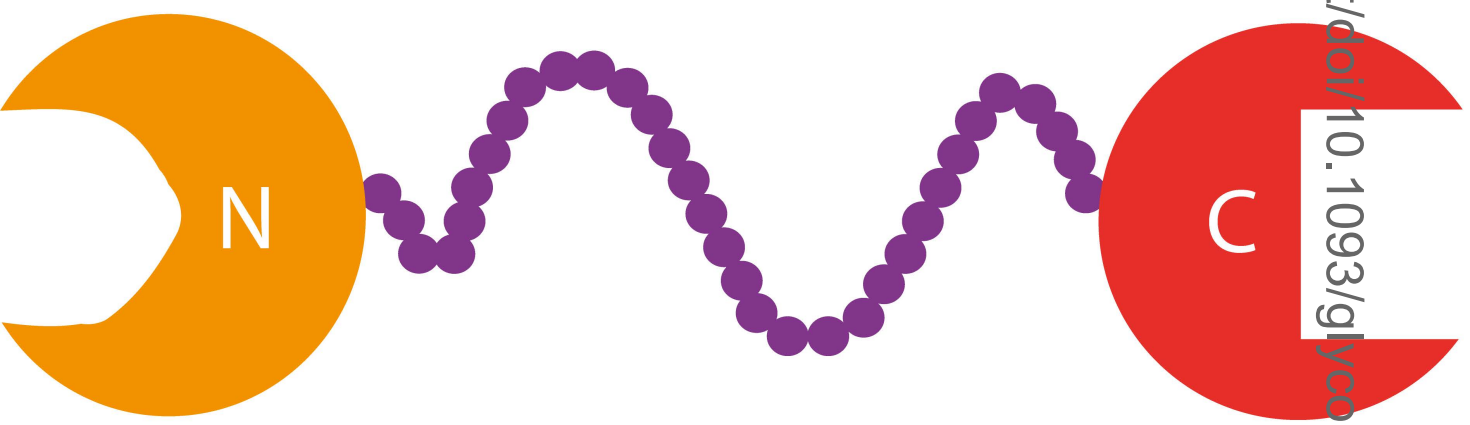

Gal-8S

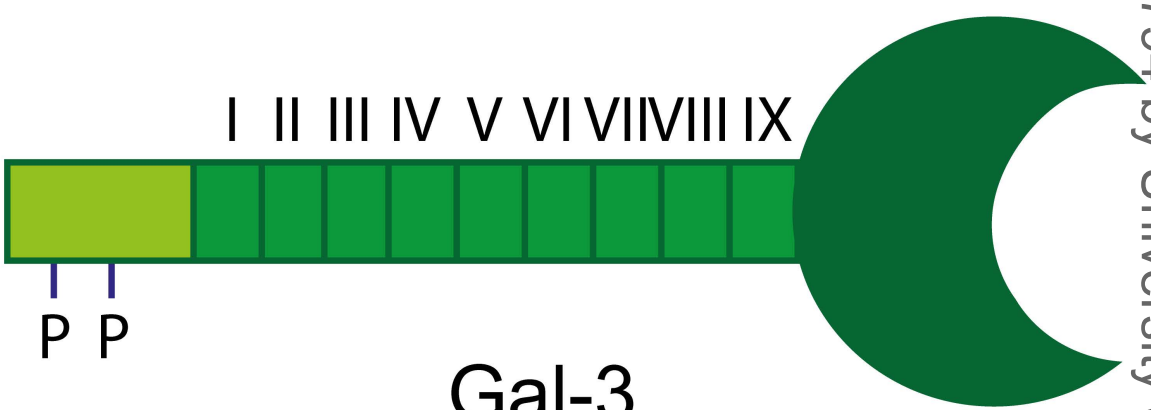

Gal-3